Fermi surface investigation of the filled skutterudite $LaRu_4As_{12}$

Klotz, J.; Götze, K.; Lorenz, V.; Prots, Y.; Rosner, H.; Harima, H.; Bochenek, L.; Henkie, Z.; Cichorek, T.; Sheikin, I.; Wosnitza, J.;

Originally published:

November 2019

Physical Review B 100(2019), 205106

DOI: https://doi.org/10.1103/PhysRevB.100.205106

Fermi-surface investigation of the filled skutterudite $LaRu_4As_{12}$

J. Klotz,[1,2] K. Götze,[1,2,*] V. Lorenz,[3] Yu. Prots,[3] H. Rosner,[3] H. Harima,[4]
L. Bochenek,[5] Z. Henkie,[5] T. Cichorek,[5] I. Sheikin,[6] and J. Wosnitza[1,2]

[1] *Hochfeld-Magnetlabor Dresden (HLD-EMFL) and Würzburg-Dresden Cluster of Excellence ct.qmat, Helmholtz-Zentrum Dresden-Rossendorf, 01328 Dresden, Germany*
[2] *Institut für Festkörper- und Materialphysik, Technische Universität Dresden, 01062 Dresden, Germany*
[3] *Max Planck Institute for Chemical Physics of Solids, 01187 Dresden, Germany*
[4] *Graduate School of Science, Kobe University, Kobe 657-8501, Japan*
[5] *Institute of Low Temperature and Structure Research, Polish Academy of Sciences, 50-950 Wrocław, Poland*
[6] *Laboratoire National des Champs Magnétiques Intenses (LNCMI-EMFL), CNRS, UGA, 38042 Grenoble, France*

(Dated: October 7, 2019)

Of all stoichiometric filled-skutterudite superconductors, $LaRu_4As_{12}$ has the highest critical field and temperature. Here, we report on a detailed Fermi-surface investigation of $LaRu_4As_{12}$ by means of de Haas-van Alphen measurements and density-functional-theory calculations. We find evidence for a nearly spherical and a multiply connected Fermi-surface sheet. The different effective masses and mass enhancements for the two sheets support two-band superconductivity, which was inferred from previous specific-heat measurements. Furthermore, quantum oscillations persist as well in the superconducting phase. We use two models to describe the additional damping, yielding energy gaps differing by a factor of five.

INTRODUCTION

The ternary transition metal pnictides with the chemical formula MT_4Pn_{12} (M = alkali metal, alkaline-earth metal, lanthanide or light actinide element; T = Fe, Ru, or Os; Pn = P, As, or Sb) crystallize in the filled skutterudite $LaFe_4P_{12}$ structure (space group $Im\bar{3}$, #204) [1, 2]. The large icosahedron cage is formed by pnictogen Pn atoms, and is centered by the electropositive element M (see upper inset Fig. 1). The transition-metal ions T are located between the cages forming a primitive cubic sublattice. As a result, the local point symmetry of an M cation is $T_h(m3)$ that does not contain four-fold rotational symmetry. Furthermore, the guest atoms M are bound loosely inside of the Pn_{12} icosahedron, whose size is much larger than the M-cation radius. This feature suggests the possible existence of local anharmonic thermal vibrations (so-called *rattling modes*) that may reduce the phononic thermal conduction and, therefore, the filled skutterudites are considered as promising thermoelectric materials. Most notably, however, the large coordination number of 12 for the guest atom M leads to sizable hybridization effects giving rise to a wide variety of strongly correlated electron phenomena [3, 4]. This subtle interplay between the M cation and the $[T_4Pn_{12}]$ framework is particularly evident in the case of rare-earth guest atoms. As shown for, e.g., the $[Ru_4As_{12}]$ sublattice, multiband superconductivity, non-Fermi-liquid behavior, conventional superconductivity, and low-lying ferromagnetic order can be realized for La [5], Ce [6], Pr [7], and Nd [8], respectively.

The most celebrated filled-skutterudite compound is $PrOs_4Sb_{12}$, currently the only known Pr-based heavy-fermion superconductor [9], that has been recently proposed as a leading candidate for hosting three-dimensional Majorana fermions [10]. Furthermore, evidence for two-band superconductivity was found in the field dependences of the electronic thermal conductivity [11–13], and an unconventional pairing mechanism seems to be in line with the critical temperature $T_c = 1.85\,\mathrm{K}$ being a factor of 2.5 higher than $T_c = 0.74\,\mathrm{K}$ of the non-$4f$-electron counterpart $LaOs_4Sb_{12}$ [14]. On the other hand, an even larger enhancement of the superconducting parameters is observed for $LaRu_4As_{12}$ with $T_c = 10.4\,\mathrm{K}$ (the upper critical field $B_{c2} \approx 10.2\,\mathrm{T}$) [5], as compared to the sister compounds $LaOs_4As_{12}$ [15] and $PrRu_4As_{12}$ [7] with $T_c = 3.2\,\mathrm{K}$ and $2.3\,\mathrm{K}$, respectively. Whereas somewhat smaller values of T_c and B_{c2} were reported for polycrystalline $LaRu_4As_{12}$ samples [16–18], both specific-heat and ^{75}As-NQR measurements are consistent with a fully gapped superconductivity [5, 19]. Upon applying pressure, T_c decreases at a rate of -0.4 K/GPa [15]. Remarkably, $LaRu_4As_{12}$ also shows evidence for multiband order parameters, as inferred from (i) the clear deviation of the zero-field electronic specific heat from the one-gap α-model behavior, (ii) the nonlinear-in-B dependence of the reduced Sommerfeld coefficient, and (iii) the positive curvature of the $B_{c2}(T)$ dependence in the vicinity of T_c [5]. Additionally, the normal-state electronic specific-heat coefficient of $\gamma = 59\ \mathrm{mJ/mol\,K^2}$ [5, 18] indicates strong electronic correlations and enhanced effective charge-carrier masses.

While other La-based filled skutterudites were experimentally shown to possess isotropic Fermi-surface (FS) sheets [14, 20–23] and/or multiply connected FSs [14, 20–24], information on the FS of $LaRu_4As_{12}$ are scarce. There are density-functional-theory (DFT) based calculations available [25], but experimental verification was

lacking.

Here, we present a detailed FS investigation of $LaRu_4As_{12}$ by combining measurements of the de Haas-van Alphen (dHvA) effect with DFT calculations using FPLO [26] and FLAPW (full potential linear augmented plane wave) [27] codes. We observe a near-spherical FS sheet along with a more complicated, multiply connected one. Effective carrier masses m^* are significantly enhanced only for the latter sheet ($m^* = 4.5 \ldots 9.3\, m_e$, with m_e being the bare electron mass), whereas for the spherical sheet we find masses of $1.5 \ldots 1.8\ m_e$. The mass-enhancement factors between the two bands clearly differ, indicating stronger electron-phonon coupling on the multiply connected sheet, which in turn renders different pairing strengths for the two bands plausible.

EXPERIMENT

Single crystals of $LaRu_4As_{12}$ were grown from elements with purities of at least 3N by mineralization in a molten Cd:As flux employing a technique detailed elsewhere [28]. They show a large residual resistivity ratio (RRR) of at least 80, evidencing high crystal quality.

Angle-dependent quantum-oscillation measurements were performed using capacitive torque magnetometry, employing 50 μm thick CuBe cantilevers. The experiments were conducted in a dilution refrigerator at a base temperature of about 30 mK. High magnetic fields were provided by an 18 T superconducting magnet at HLD and a 34 T resistive magnet at the LNCMI-Grenoble.

High-resolution x-ray synchrotron powder diffraction was performed at beamline ID22 of the European Synchrotron Radiation Facility (ESRF) Grenoble, France. The experimental diffraction data were recorded using a wavelength of 0.40074 Å at temperatures of 10, 80, 140, and 295 K. All crystallographic calculations were performed using the program package WinCSD [29].

RESULTS AND DISCUSSION

Fermi surface and band structure

Figure 1 shows a typical torque signal for $LaRu_4As_{12}$ taken at an angle $\Theta_{0\bar{1}1} = 2°$. Throughout this paper, all angles are measured from the crystallographic [100] axis. At fields lower than about 10 T, a clear hysteresis and a strong peak effect appear in the superconducting mixed state [31]. The onset of the peak effect slightly varies between up and down sweep. From the average onset, we determine $B_{c2} \approx 9.8(1)$ T [32], in good agreement with previously reported values [5, 18]. In addition, quantum oscillations are visible at higher fields (see inset of Fig. 1). When rotating the field away from $B \parallel [100]$, these oscillations become more pronounced, as shown in the inset of Fig. 2. The main panel shows the corresponding frequency spectrum obtained by Fourier transformation. Three fundamental dHvA frequencies labeled α, δ, and ϵ, and two higher harmonics of δ are clearly visible.

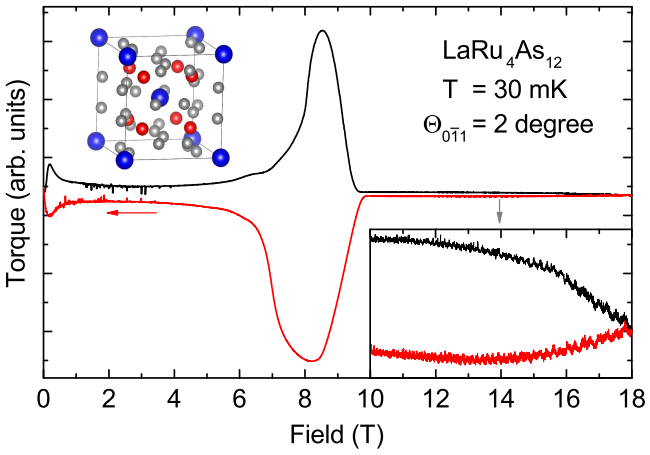

FIG. 1. Raw torque signal near $B \parallel a$. Black and red curves represent up- and down-sweep of the magnetic field, respectively. Lower inset: Zoom into the high-field region showing quantum oscillations. The torque oscillations shown here are relatively small due to the small angle between magnetic field and the [100] direction. Upper inset: Unit cell for $LaRu_4As_{12}$. Blue: La, red: Ru, grey: As; created using [30].

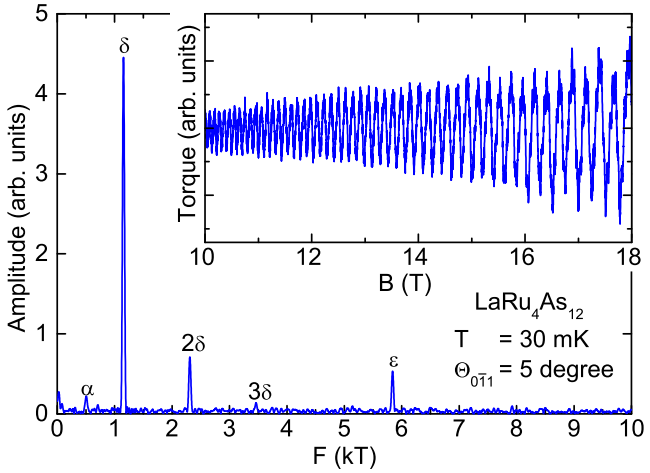

FIG. 2. Inset: Torque signal after subtraction of a second-order background polynomial. Main panel: Corresponding frequency spectrum obtained by Fourier transformation.

By repeating field sweeps at different angles, we obtained the angular dependence of the dHvA frequencies shown together with calculated frequencies (see below) in Fig. 3. Altogether, we find seven fundamental frequency branches, denoted as α, β, γ, δ, ϵ, ϕ, and ψ. Only δ is observed for all crystallographic directions with little changes in frequency, thus evidencing a nearly spherical FS sheet. The remaining frequencies, on the other hand, appear only for smaller angular ranges, hinting at the presence of a more complicated, multiply connected FS

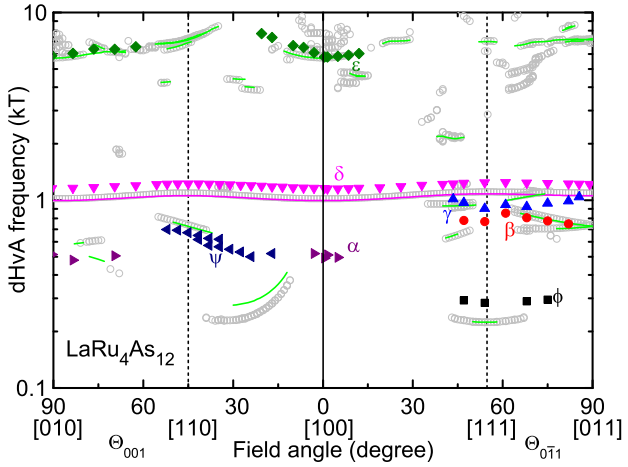

FIG. 3. Angular dependence of experimental (large symbols) and calculated dHvA frequencies (lines: FPLO code; small, open symbols: KANSAI code). Left panel: Rotation from $B \parallel [100]$ to $B \parallel [010]$. Note that the dHvA frequencies are not symmetric around the [110] axis because the $Im\bar{3}$ structure does not possess any corresponding symmetry element. Right panel: Rotation from $B \parallel [100]$ to $B \parallel [011]$.

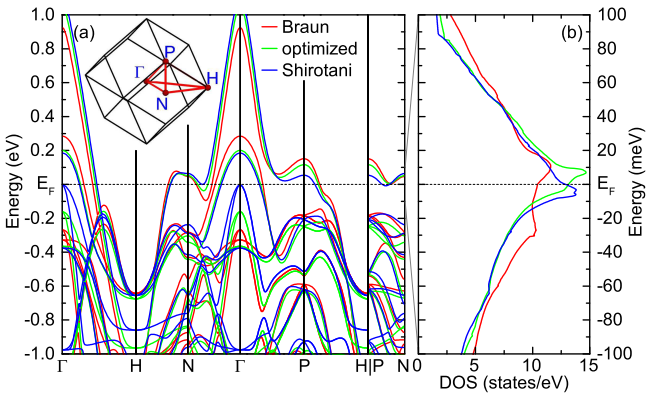

FIG. 4. Influence of y and z atomic positions. (a) Calculated band-structure (using the LDA exchange functional) for the positions measured by Braun and Jeitschko [2] (red), Shirotani et al. (private communication in [25]) (blue), and optimized by FPLO (green). (b) Corresponding DOS. For clarity, the graph only shows a narrow region around E_F.

sheet. Note that the $Im\bar{3}$ crystal structure is characterized by the absence of symmetry elements around the [110] axis. Hence, the experimental dHvA frequencies are not expected to be symmetric around the [110] axis when rotating the crystal around the [001] axis. Experiments at higher magnetic fields up to 34 T did not reveal any additional frequency branches.

In order to determine the FSs corresponding to the experimental dHvA frequencies, we conducted DFT calculations for $LaRu_4As_{12}$ using the FPLO code (version 15.02-50) [26]. To approximate the exchange and correlation potential, we used the local density approximation (LDA) of Perdew and Wang [33] and a scalar-relativistic setting. We used a $24\times24\times24$ k mesh for calculating the self-consistent density and an 8 times denser grid for the FSs. Additional calculations were performed using the KANSAI code, based on a FLAPW method using LDA [27].

While the value of $a = 8.5081$ Å was reported from various sources, the relative internal As positions (0, y, z) reported by different groups do not match. Experimental data from Braun and Jeitschko ($y = 0.15474$ and $z = 0.34556$) [2] significantly differ from those measured by Shirotani et al. ($y = 0.147$ and $z = 0.350$, private communication in Ref. [25]) and those calculated by Ram et al. ($y = 0.1503$ and $z = 0.3501$) [25]. We also conducted a numerical optimization of the internal atomic positions using FPLO and obtained $y = 0.1510$ and $z = 0.3493$. When comparing band structures calculated using the parameters found by Braun, Shirotani, and FPLO, clear differences become obvious, as shown in Fig. 4(a). Since many of the energy shifts and slight changes in the bands' shapes occur near the Fermi energy (E_F), they greatly influence the corresponding FS sheets. Additionally, all three calculations produce a peak in the density of states (DOS) near E_F, but the peak position and value strongly differ. Thus, high-resolution low-temperature structural data are vital for achieving reliable band-structure and FS calculations. Consequently, we carried out synchrotron x-ray-diffraction measurements at 10 K, yielding $a = 8.49562(1)$ Å, $y = 0.1497(3)$, and $z = 0.3505(3)$.

For all further calculations, we used the experimentally refined crystallographic data and a full-relativistic setting taking spin-orbit coupling into account. Because of the centrosymmetric crystal structure of $LaRu_4As_{12}$, the spin-orbit coupling does not lift the spin degeneracy of the bands. For simplicity, we will discuss degenerate bands as single bands carrying the DOS of both spin channels. The outcome of the calculations is depicted in Fig. 5. There are two bands crossing E_F, labeled 175 and 176 [see Fig. 5(a)]. Band 175 crosses E_F almost isotropically around the Γ point of the Brillouin zone (BZ), leading to a nearly spherical FS sheet [Fig. 5(c)]. In contrast, band 176 crosses E_F multiple times between the high-symmetry points, and lies within $E_F \pm 100$ meV in a large portion of the BZ. Consequently, the FS arising from band 176 is multiply connected, possessing many holes and curved features. For clarity, Figs. 5(d)-(f) show this FS from different perspectives. Furthermore, the flat dispersion of band 176 in some parts of the BZ produces a peak of the DOS D lying only 4.5 meV above E_F, as shown in Figs. 4(b) and 5(b). Band 176 contributes 96% of $D(E_F) = 13.6$ states/eV. Using the relation

$$\gamma_{calc} = \frac{\pi^2 k_B^2}{3} D(E_F), \qquad (1)$$

where k_B denotes Boltzmann's constant, we obtain the corresponding Sommerfeld coefficient $\gamma_{calc} = 32.1\ \mathrm{mJ/mol\,K^2}$.

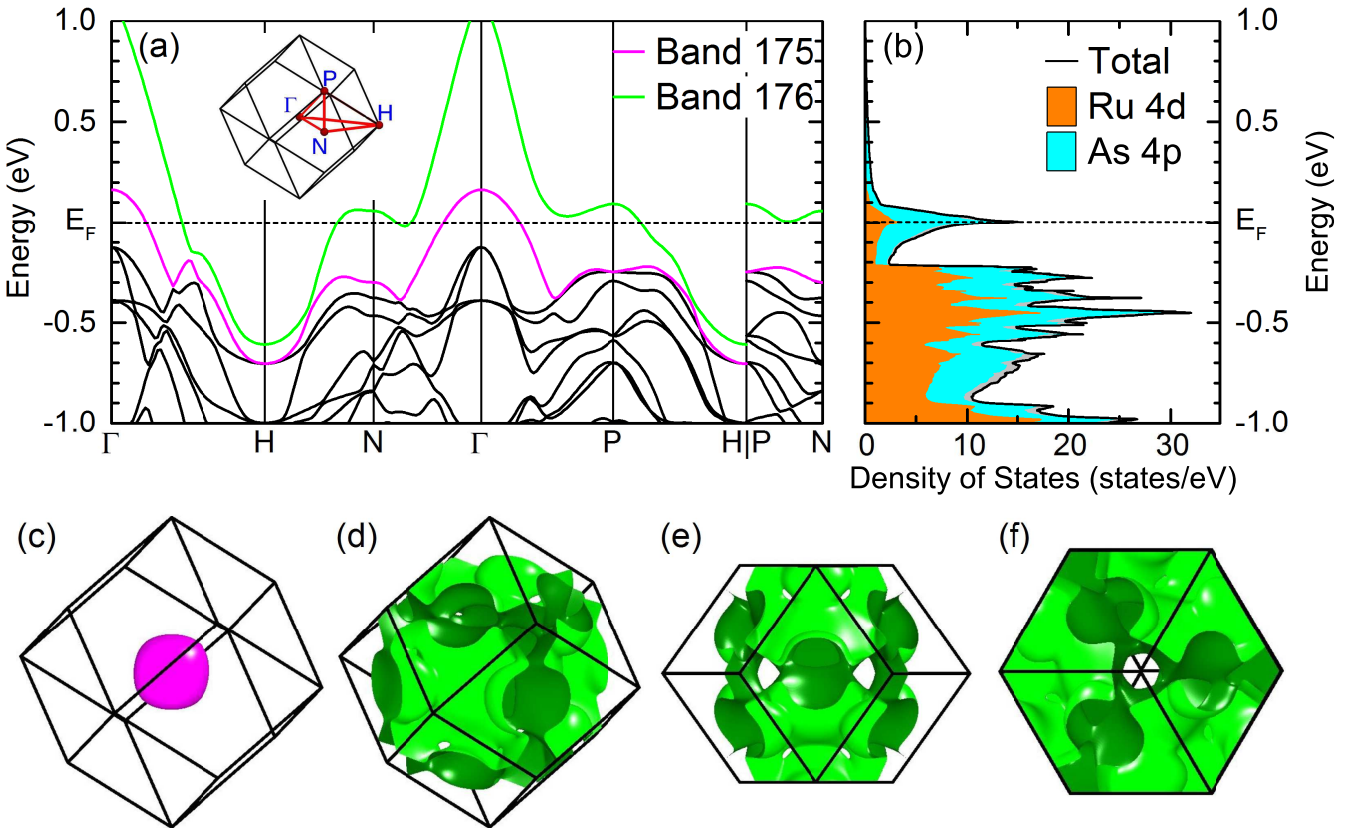

FIG. 5. (a) Calculated band structure of $LaRu_4As_{12}$ along high-symmetry lines of the BZ. Bands 175 (magenta) and 176 (green) cross E_F. (b) Calculated DOS near E_F. Shaded areas mark the contributions of Ru-4*d* (orange) and As-4*p* states (cyan). (c) Calculated FS of band 175. (d)-(f) Calculated FS of band 176, shown from different perspectives: (d) identical to the sketch in (a), (e) parallel to the [110] axis, and (f) parallel to the [111] axis. All results in this figure were obtained using the FPLO code.

The band-structure calculations in [25] using a non-local version of the exchange-correlation functional and slightly lower values for y and z yielded similar results to those presented here. However, the details of the band structure and the DOS close to E_F are very sensitive to changes in the structural parameters as we demonstrated in Fig. 4, and we, therefore, believe that calculations using low-temperature crystallographic data allow for a more accurate picture of the band structure in $LaRu_4As_{12}$.

Figure 3 shows calculated and experimental dHvA frequencies. Virtually the same results were obtained for the calculated frequencies using the FPLO and the KANSAI code. The nearly spherical FS of band 175 possesses only one extremal cross-section for every field direction, resulting in a single-frequency branch spanning the full angular range. This branch is in excellent qualitative agreement with the experimental branch δ, offset by only 150 T. Conversely, the multiply connected FS of band 176 creates a wealth of frequency branches, some of which exist only for narrow angular ranges. Most remaining experimental frequency branches are in good agreement with calculated branches of band 176, with only α not explained by theory. We point out that slight deviations of the structural data leads to altered results: using the Shirotani internal coordinates leads to the absence of the theoretical frequency branch supporting ψ, but features a branch explaining α.

Effective masses

Effective masses m^* were determined from the temperature dependence of the dHvA oscillation amplitudes, which were measured for temperatures between 50 and 900 mK at two different angles. According to the Lifshitz-Kosevich formula, the temperature dependence is proportional to the temperature damping factor R_T, given by $R_T = x/\sinh x$, where $x = \alpha T m^*/B$ and $\alpha = 14.69$ T/K [34]. Here, m^* represents the effective mass given in multiples of the bare electron mass m_e. Figure 6 shows the fit of the temperature dependence of the oscillatory amplitudes by this formula, yielding m^* as fit parameter. Table I summarizes experimental effective masses together with band masses, m_b, calculated by

			Experiment		Calculation[a]		λ
Branch	Band	Angle	F (kT)	m^* (m_e)	F (kT)	m_b (m_e)	$m^*/m_b - 1$
α	?	$\Theta_{0\bar{1}1} = 5°$	0.51	4.5(2)			
δ	175	$\Theta_{0\bar{1}1} = 5°$	1.15	1.5(1)	0.998	0.69	1.2
ϵ	176	$\Theta_{0\bar{1}1} = 5°$	5.39	9.3(3)	5.775	2.82	2.3
	176	$\Theta_{001} = 42°$			0.027	1.29	
ψ_1	176	$\Theta_{001} = 42°$	0.55	5.5(3)	0.704	1.53	2.6
ψ_2	176	$\Theta_{001} = 42°$	0.65	5.6(6)	0.704	1.53	2.7
δ	175	$\Theta_{001} = 42°$	1.22	1.8(1)	1.057	0.75	1.4
	176	$\Theta_{001} = 42°$			7.43	4.7	
	176	$\Theta_{001} = 42°$			7.55	5.2	

[a] Effective mass calculations using the FLAPW based KANSAI code yielded the same results with a maximum deviation of 5%.

TABLE I. Experimental and calculated (FPLO) dHvA frequencies and effective masses of $LaRu_4As_{12}$. Branch assignments and angles refer to Fig. 3.

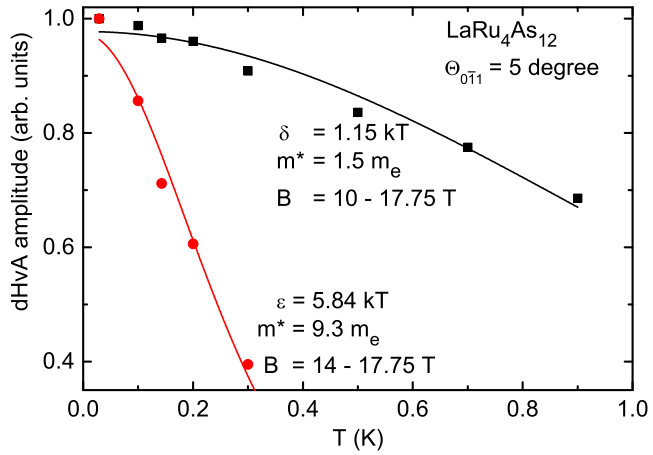

FIG. 6. Temperature-dependent amplitudes, taken at $\Theta_{0\bar{1}1} = 5°$, with fit lines determined by use of the Lifshitz-Kosevich formula.

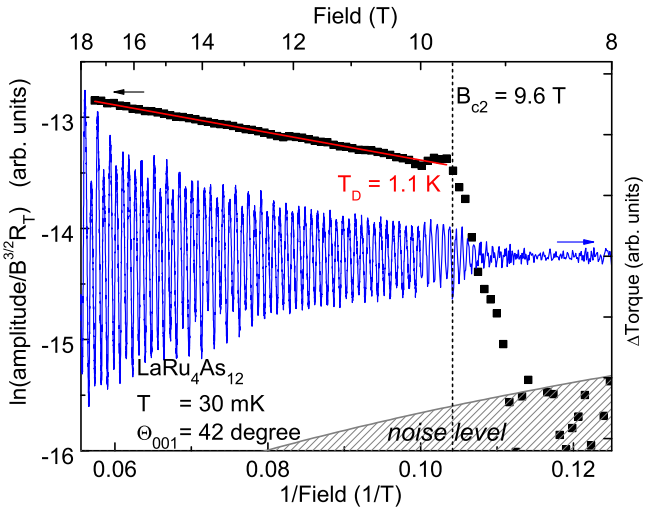

FIG. 7. Field dependence of dHvA signals at $\Theta_{001} = 42°$. The blue curve shows the torque signal after subtraction of a non-oscillatory background. Black symbols represent a Dingle plot of the amplitudes for $\delta = 1.216$ kT, the red line shows a linear fit to the data above the superconducting phase. B_{c2} was determined by the onset of the peak effect. In order to reduce interference from smaller frequencies, we averaged over four periods per data point.

taking the derivative dF/dE. Due to many-body interactions, the experimental m^* is enhanced compared to m_b by a mass-enhancement factor defined as $\lambda = m^*/m_b - 1$. For the near-spherical band 175, m_b, m^*, and λ are clearly smaller than for band 176. For both angles investigated, m^* for δ lies at 1.5 and 1.8 m_e, resulting in $\lambda = 1.2$ and 1.4, respectively. On the other hand, the frequencies arising from the multiply connected FS sheet feature higher masses of 4.5 to 9.3 m_e, yielding $\lambda = 2.3$-2.7. Hence, consistent with the large specific-heat jump at T_c reported in Ref. [5], there are strong many-body interactions, which we assume are mainly due to electron-phonon coupling. The significant difference in λ for the two bands is in line with the proposed two-gap superconductivity with different Δ and B_c. Note that the mass enhancement deduced from the Sommerfeld coefficients via $\lambda = \gamma_{exp}/\lambda_{calc} - 1$ yields only $\lambda = 0.84$, which is smaller than the enhancements for the different orbits. This means that the calculated DOS is overestimated or the band masses are underestimated by a factor of two. This is surprising since the mass enhancements of the Sommerfeld coefficient is expected to be a weighted average of the mass enhancements of the electronic orbits. A similar behavior was also observed in other isoelectronic compounds, such as $LaOs_4P_{12}$ [23, 35]. Since the λ values deduced from our dHvA experiments are averaged over extremal FS orbits, smaller mass enhancements for others parts of the FS might be a possible explanation for the discrepancy of λ obtained from dHvA and specific-heat measurements.

Damping in the normal and superconducting state

In the next step, we analyze the field dependence of the δ frequency, which produces the largest dHvA amplitudes in our measurements. The field dependence of the dHvA oscillation amplitudes A, measured by torque, is given by $A \propto R_T R_D R_{SC} B^{3/2}$ [34],[36]. Here, R_T, R_D, and R_{SC} are damping factors representing the impact of finite temperature, impurity scattering, and additional amplitude reduction in the superconducting phase, respectively. The so-called Dingle damping factor, R_D, for a fundamental dHvA frequency can be written as $R_D = \exp(-\alpha m_b T_D/B)$. The Dingle temperature, T_D, depends on the scattering rate, $1/\tau$, via $T_D = \hbar/(2\pi k_B \tau)$. $\hbar$ is the reduced Planck constant. Note that this damping factor depends on the bare band mass m_b, not on the effective mass m^* [37].

In order to disentangle the different damping factors, we initially focus on the normal state, where $R_{SC} \equiv 1$. Since R_T can be calculated using the previously determined m^*, creating a so-called Dingle plot, $\ln(A/[R_T B^{3/2}])$ vs. $1/B$, allows to determine T_D from a linear fit, as shown in Fig. 7. Indeed, the amplitudes in this plot behave nearly perfectly linear, with small deviations due to interference with other frequencies. From a fit between $B_{c2} \approx 9.6$ T [38] and 18 T, we deduce $T_D = 1.1$ K, indicating the high quality of our single crystal.

While the amplitude behaves nearly linear in the normal phase, it quickly drops in the superconducting state. The opening of the superconducting energy gap causes the FS to vanish since $LaRu_4As_{12}$ is a fully gapped superconductor [5, 19]. Hence, it may seem surprising that dHvA oscillations are detected inside the superconducting state. However, in the Shubnikov phase of a type-II superconductor, normal-conducting flux lines can penetrate the material. Electrons can tunnel between the flux lines and accomplish the cyclotron motion necessary for the dHvA effect. Further decreasing magnetic field increases the spacing between the flux lines and subsequently the tunneling probability. Thus, dHvA oscillations are damped more strongly inside the superconducting phase, which gets accounted for by R_{SC}. The field inhomogeneity introduced by the flux lines causes an additional damping, which we do not take into account since it is usually much smaller than R_{SC} [39, 40].

There are multiple representations of R_{SC}, based on different theoretical approaches (for an overview, see Ref. [39] and references therein). Here, we compare our data to the theories of Maki, Stephen, Wasserman, and Springford (MSWS) [41–44] and of Miyake, Miller, and Györffy (MMG) [45, 46]. Both theories were applied to analyze numerous compounds in the past. Although both may provide a good qualitative agreement to experiment, they often result in gap values differing by a factor larger than four, e. g., in MgB_2 [47], V_3Si, or $NbSe_2$ [39]. Inconsistently, MMG allows a better approximation of the experimental gap only in MgB_2 and V_3Si, whereas MSWS works better for $NbSe_2$. For fundamental dHvA frequencies F, in a field B smaller than the critical field B_{c2}, these theories yield:

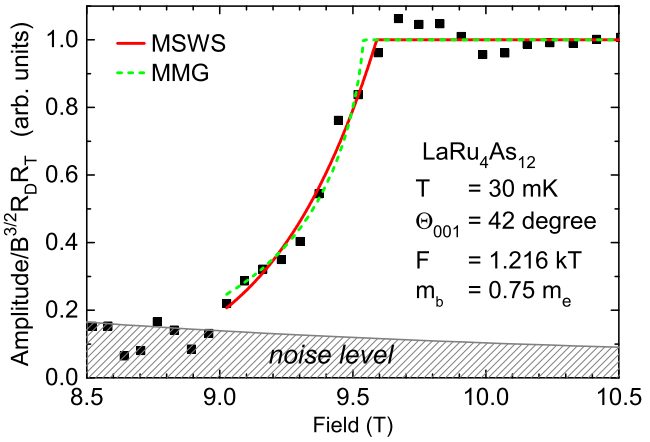

FIG. 8. Field dependence of the oscillation amplitude reduction within the superconducting phase. Symbols indicate dHvA oscillation amplitudes rescaled by R_D and R_T. Lines are fits of different theoretical models to the data (see text).

$$R_{SC} = \exp\left(-\sqrt{B/(16\pi F)}\varphi^2\right) \quad \text{(MSWS)}, \qquad (2)$$

$$R_{SC} = \varphi K_1(\varphi) \quad \text{(MMG)}, \qquad (3)$$

where $\varphi = (2\pi m_b \Delta)/(\hbar e B)$, K_1 is the modified Bessel function, and Δ the superconducting energy gap. We use the expression

$$\Delta(B) = \Delta(0)\sqrt{1 - B/B_{c2}} \qquad (4)$$

to describe the superconducting gap at finite fields. A more recent third theory by Yasui and Kita (YK) [48] derives an expression $R_{SC} = \exp\left[\Gamma\varphi^2/(2\pi)\right]$, with $\Gamma = 0.125$. Only the pre-factor of φ^2 in the exponent differs from Eq. (2), leading to qualitatively identical behavior, and in our case to gap values differing by 10%. Therefore, we will not consider YK separately.

A fit of Eqs. (2) and (3) to the normalized dHvA amplitudes is shown in Fig. 8. Here, both Δ and B_{c2} were free parameters for the fit, leading to a very good description of the decaying amplitudes by both models. Slight deviations between models and experiment may arise from interference of the strongly changing non-oscillatory background signal caused by the peak effect. We obtain $\Delta = 10.4$ meV and $B_{c2} = 9.59$ T from MSWS, as well as $\Delta = 2.06$ meV and $B_{c2} = 9.54$ T from MMG. Hence, the MSWS model predicts a band gap which seems to be unrealistically large. It is five times larger than the gap derived from the MMG model, and also more than four times larger than the gaps $\Delta_1 = 2.35$ meV and

Δ_2 = 1.67 meV estimated from specific-heat measurements [5]. Since the frequency δ investigated in this analysis relates to the band with the smaller λ and the smaller DOS, we assume it most likely possesses the smaller band gap Δ_2. Thus, the MMG model overestimates the gap by only about 23%, and provides a better approximation than MSWS, similar as observed in MgB_2 [47] and V_3Si [39]. However, we note that when using the torque method, there might be an additional damping possibly related to flux-line dynamics, as has been observed in YNi_2B_2C [40, 49]. Since both the MSWS and the MMG model yield largely different energy gaps for several compounds, and the damping in the superconducting state may be dependent on the measurement method, more theoretical and experimental work is required to fully understand quantum oscillations in the Shubnikov phase of type-II superconductors.

Comparison to iso-electronic skutterudites

The LaT_4Pn_{12} family (where T = Fe, Ru, and Os; Pn = P, As, and Sb) forms a total of nine iso-electronic compounds, since all T and Pn elements possess an identical number of outer-shell d and p electrons, respectively. In $LaFe_4As_{12}$ and $LaFe_4Sb_{12}$, a high DOS is presumably responsible for their nearly or weakly ferromagnetic behavior, respectively [58–61]. All other LaT_4Pn_{12} family members are superconducting (see [62] and references therein). To the best of our knowledge, our report on $LaRu_4As_{12}$ completes the experimental FS data of the superconducting members [14, 20–24, 57, 61]. When comparing these seven compounds, we note a general similarity of the band structures, which is not surprising for iso-electronic materials. All compounds possess two bands crossing E_F. One of them (band 175 in $LaRu_4As_{12}$) leads to a fairly isotropic FS sheet around Γ, except for $LaRu_4P_{12}$, where the corresponding band stays just below E_F at the Γ point [24]. Additionally, a second band (corresponding to band 176 in $LaRu_4As_{12}$) exists, which lies close to E_F in some regions of the BZ. Due to slight differences between the electrostatic potentials and internal positions of the T and Pn atoms, the shape of this band slightly differs. These small differences influence the positions and number of crossings of E_F, thus creating a variety of different FS sheets within the LaT_4Pn_{12} family [14, 20–24, 57, 61].

Table II shows the T_c's of all superconducting members of the LaT_4Pn_{12} family, along with experimental and calculated Sommerfeld coefficients and effective masses, and the inferred mass enhancements. For better comparability, all values of $\gamma_{\rm exp}$ were taken from a systematic study of Matsuhira et al. [50] and are largely in good agreement with other studies [5, 17, 35, 51]. Note, however, that there are discrepancies by up to a factor of 2 with other reports for $LaRu_4P_{12}$ [24] and $LaOs_4As_{12}$ [54]. In some cases, we used Eq. (1) to obtain $\gamma_{\rm calc}$ from the reference. All LaT_4Pn_{12} superconductors have a moderate mass enhancement inferred from the Sommerfeld coefficient, obtained via $\lambda_\gamma = \gamma_{\rm exp}/\gamma_{\rm calc} - 1$ = 0.33-0.84. For $LaOs_4P_{12}$ and $LaRu_4As_{12}$, this mass enhancement is clearly smaller than the values obtained for both bands. The largest values for λ_γ, $\lambda_{\rm sp}$, and $\lambda_{\rm mc}$ are found in the compounds with the largest T_c, $LaRu_4As_{12}$. However, there is no obvious trend between T_c and the different λ for the remaining compounds. Furthermore, the trend of greatly increased T_c for compounds with Ru on the T site compared to their Os counterparts is not reflected in any other FS property.

SUMMARY

We performed a comprehensive FS investigation of the filled-skutterudite superconductor $LaRu_4As_{12}$ by combining dHvA measurements and FPLO-and FLAPW-based DFT calculations. Experimental and calculated data are in excellent agreement, revealing the presence of two bands at E_F. One of the bands contributes to only 4% of the DOS at E_F, creating a nearly isotropic FS sheet with low effective masses (m^* = 1.5-1.8 m_e) and moderate mass enhancements (λ = 1.2-1.4). The main DOS contribution comes from the second band, producing a multiply connected FS sheet with elevated effective masses (m^* = 4.5-9.3 m_e) and higher mass enhancements (λ = 2.3-2.7). The presence of two bands with largely different DOS contributions, effective masses, and mass enhancements are in line with multiband superconductivity in $LaRu_4As_{12}$. Additionally, we were able to detect quantum oscillations in the superconducting state. We used two theoretical models describing the additional damping below B_{c2} for fitting to the experimental data. The deduced superconducting gap for the MMG model slightly overestimates the experimental value, whereas the MSWS model yields a gap five times larger.

ACKNOWLEDGMENTS

We acknowledge support from the DFG through the Würzburg-Dresden Cluster of Excellence on Complexity and Topology in Quantum Matter – *ct.qmat* (EXC 2147, project-id 39085490), the ANR-DFG grant 'FermiNESt', and by HLD at HZDR and LNCMI-CNRS, which are both members of the European Magnetic Field Laboratory (EMFL). We would like to thank the ESRF for provision of beamtime at the ID22 beamline. K.G. acknowledges support from the DFG within GRK 1621.

	T_c (K)	$\gamma_{\rm exp}$ [50] (mJ/mol K^2)	$\gamma_{\rm calc}$ (mJ/mol K^2)	λ_γ	$m^*_{\rm sp}$ (m_e)	$\lambda_{\rm sp}$	$m^*_{\rm mc}$ (m_e)	$\lambda_{\rm mc}$	Refs.
$LaFe_4P_{12}$	4.1	52	31	0.68	2.3	0.61	7.0-8.8	0.76-1.3	[20, 51]
$LaRu_4P_{12}$	7.2	29 (44 [24])	19	0.53	–	–	2.9-11.8	0.55-2.1	[17, 24, 52]
$LaOs_4P_{12}$	2.0	20	15	0.33	1.1	0.97	4.7	1.4	[23, 35, 53]
$LaRu_4As_{12}$	10.45	59	32.1	0.84	1.5	1.2	4.5-9.3	2.3-2.7	[5], this work
$LaOs_4As_{12}$	3.2	49 (93 [54])	?	?	1.3	0.52	2.0-3.3	1.1-1.3	[15, 22, 54, 55]
$LaRu_4Sb_{12}$	3.6	47	?	?	1.7	?	1.1-1.4	?	[21, 50, 56]
$LaOs_4Sb_{12}$	0.74	54	36	0.50	0.7	0.58	2.5-4.1	1.8-2.5	[14, 57]

TABLE II. Comparison of the superconducting LaT_4Pn_{12} members (T = Fe, Ru, and Os; Pn = P, As, and Sb) with respect to properties determined by specific-heat and dHvA measurements, band-structure calculations, and their T_c. The index 'sp' labels properties measured for the near-spherical FS sheet with $B \parallel [100]$. The index 'mc' represents properties of the multiply connected sheets for various directions. For $LaOs_4As_{12}$ and $LaOs_4Sb_{12}$, this includes the near-cubic sheets. All experimental values of $\gamma_{\rm exp}$ were taken from Ref. [50] (see text for further information). For $LaOs_4As_{12}$, we compared to calculated band masses of $4f$-localized $PrOs_4As_{12}$, which is equivalent to $LaOs_4As_{12}$ calculations with slightly different lattice parameters [22].

* K.Gotze@warwick.ac.uk; Present address: Department of Physics, University of Warwick, Coventry, CV4 7AL, United Kingdom

[1] W. Jeitschko and D. Braun, Acta Cryst. **33**, 3401 (1977).
[2] D. J. Braun and W. Jeitschko, J. Solid State Chem. **32**, 357 (1980).
[3] H. Sato, H. Sugawara, Y. Aoki, and H. Harima, *Handbook of Magnetic Materials*, edited by B. K. H. J., Vol. 18 (North-Holland, Amsterdam, 2009) p. 1.
[4] M. B. Maple, Z. Henkie, R. E. Baumbach, T. A. Sayles, N. P. Butch, P.-C. Ho, T. Yanagisawa, W. M. Yuhasz, R. Wawryk, T. Cichorek, and A. Pietraszko, J. Phys. Soc. Jpn. **77**, 7 (2008).
[5] L. Bochenek, R. Wawryk, Z. Henkie, and T. Cichorek, Phys. Rev. B **86**, 060511 (2012).
[6] R. E. Baumbach, P. C. Ho, T. A. Sayles, M. B. Maple, R. Wawryk, T. Cichorek, A. Pietraszko, and Z. Henkie, J. Phys.: Condens. Matter **20**, 075110 (2008).
[7] T. A. Sayles, R. E. Baumbach, W. M. Yuhasz, M. B. Maple, L. Bochenek, R. Wawryk, T. Cichorek, A. Pietraszko, Z. Henkie, and P.-C. Ho, Phys. Rev. B **82**, 104513 (2010).
[8] A. Rudenko, Z. Henkie, and T. Cichorek, Solid State Commun. **242**, 21 (2016).
[9] E. D. Bauer, N. A. Frederick, P.-C. Ho, V. S. Zapf, and M. B. Maple, Phys. Rev. B **65**, 100506 (2002).
[10] V. Kozii, J. W. F. Venderbos, and L. Fu, Sci. Adv. **2**, e1601835 (2016).
[11] G. Seyfarth, J. P. Brison, M.-A. Masson, J. Flouquet, K. Izawa, Y. Matsuda, H. Sugawara, and H. Sato, Phys. Rev. Lett. **95**, 107004 (2005).
[12] G. Seyfarth, J. P. Brison, M.-A. Masson, D. Braithwaite, G. Lapertot, and J. Flouquet, Phys. Rev. Lett. **97**, 236403 (2006).
[13] R. W. Hill, S. Li, M. B. Maple, and L. Taillefer, Phys. Rev. Lett. **101**, 237005 (2008).
[14] H. Sugawara, S. Osaki, S. R. Saha, Y. Aoki, H. Sato, Y. Inada, H. Shishido, R. Settai, Y. Ōnuki, H. Harima, and K. Oikawa, Phys. Rev. B **66**, 220504 (2002).
[15] I. Shirotani, K. Ohno, C. Sekine, T. Yagi, T. Kawakami, T. Nakanishi, H. Takahashi, J. Tang, A. Matsushita, and T. Matsumoto, Physica B **281-282**, 1021 (2000).
[16] I. Shirotani, T. Uchiumi, K. Ohno, C. Sekine, Y. Nakazawa, K. Kanoda, S. Todo, and T. Yagi, Phys. Rev. B **56**, 7866 (1997).
[17] T. Uchiumi, I. Shirotani, C. Sekine, S. Todo, T. Yagi, Y. Nakazawa, and K. Kanoda, J. Phys. Chem. Solids **60**, 689 (1999).
[18] T. Namiki, C. Sekine, K. Matsuhira, M. Wakeshima, and I. Shirotani, J. Phys. Soc. Jpn. **77**, 336 (2008).
[19] M. Shimizu, H. Amanuma, K. Hachitani, H. Fukazawa, Y. Kohori, T. Namiki, C. Sekine, and I. Shirotani, J. Phys. Soc. Jpn. **76**, 104705 (2007).
[20] H. Sugawara, Y. Abe, Y. Aoki, H. Sato, M. Hedo, R. Settai, Y. Ōnuki, and H. Harima, J. Phys. Soc. Jpn. **69**, 2938 (2000).
[21] T. D. Matsuda, K. Abe, F. Watanuki, H. Sugawara, Y. Aoki, H. Sato, Y. Inada, R. Settai, and Y. Ōnuki, Physica B **312-313**, 832 (2002).
[22] P.-C. Ho, J. Singleton, M. B. Maple, H. Harima, P. A. Goddard, Z. Henkie, and A. Pietraszko, New J. Phys. **9**, 269 (2007).
[23] H. Sugawara, Y. Iwahashi, K. Magishi, T. Saito, K. Koyama, H. Harima, D. Kikuchi, H. Sato, T. Endo, R. Settai, and Y. Ōnuki, Phys. Rev. B **79**, 035104 (2009).
[24] S. R. Saha, H. Sugawara, Y. Aoki, H. Sato, Y. Inada, H. Shishido, R. Settai, Y. Ōnuki, and H. Harima, Phys. Rev. B **71**, 132502 (2005).
[25] S. Ram, V. Kanchana, and M. C. Valsakumar, J. Appl. Phys. **115**, 093903 (2014).
[26] K. Koepernik and H. Eschrig, Phys. Rev. B **59**, 1743 (1999).
[27] I. Sakamoto, G. F. Chen, S. Ohara, H. Harima, and S. Maruno, J. Alloys Cmpd. Proceedings of the 4th International Conference on f-Elements, **323-324**, 623 (2001).
[28] Z. Henkie, M. B. Maple, A. Pietraszko, R. Wawryk, T. Cichorek, R. E. Baumbach, W. M. Yuhasz, and P.-C. Ho, J. Phys. Soc. Jpn. **77**, 128 (2008).
[29] L. Akselrud and Yu. Grin, J. Appl. Cryst. **47**, 803 (2014).
[30] K. Momma and F. Izumi, J. Appl. Cryst. **44**, 1272 (2011).
[31] The minute hysteresis visible above B_{c2} up to highest fields presumably is an experimental artifact.
[32] Note that in Ref. [5], the critical field for $B \parallel [100]$ was about 4% smaller than for $B \parallel [110]$ at 3 K. Assuming a similar anisotropy at lowest temperatures, we estimate $B_{c2} \approx 9.8$ T for $B \parallel [100]$.

[33] J. P. Perdew and Y. Wang, Phys. Rev. B **45**, 13244 (1992).

[34] D. Shoenberg, *Magnetic Oscillations in Metals* (Cambridge University Press, Cambridge, UK, 1984).

[35] K. Matsuhira, Y. Doi, M. Wakeshima, Y. Hinatsu, K. Kihou, C. Sekine, and I. Shirotani, Physica B **359-361**, 977 (2005).

[36] Note that we omitted the spin-damping factor R_S because it is not field dependent, and, therefore, not relevant here.

[37] A. Carrington, Rep. Prog. Phys. **74**, 124507 (2011).

[38] Note that both the onset of the peak effect and the additional damping set in below 9.6 T, which is slightly smaller than the critical field of 10.2 T reported for $B \parallel [110]$.

[39] T. J. B. M. Janssen, C. Haworth, S. M. Hayden, P. Meeson, M. Springford, and A. Wasserman, Phys. Rev. B **57**, 11698 (1998).

[40] J. Nössler, R. Seerig, S. Yasin, M. Uhlarz, S. Zherlitsyn, G. Behr, S.-L. Drechsler, G. Fuchs, H. Rosner, and J. Wosnitza, Phys. Rev. B **95**, 014523 (2017).

[41] K. Maki, Phys. Rev. B **44**, 2861 (1991).

[42] M. J. Stephen, Phys. Rev. B **43**, 1212 (1991).

[43] M. J. Stephen, Phys. Rev. B **45**, 5481 (1992).

[44] A. Wasserman and M. Springford, Physica B **194-196**, 1801 (1994).

[45] K. Miyake, Physica B **186-188**, 115 (1993).

[46] P. Miller and B. L. Györffy, J. Phys.: Condens. Matter **7**, 5579 (1995).

[47] J. D. Fletcher, A. Carrington, S. M. Kazakov, and J. Karpinski, Phys. Rev. B **70**, 144501 (2004).

[48] K. Yasui and T. Kita, Phys. Rev. B **66**, 184516 (2002).

[49] T. Terashima, C. Haworth, H. Takeya, S. Uji, H. Aoki, and K. Kadowaki, Phys. Rev. B **56**, 5120 (1997).

[50] K. Matsuhira, C. Sekine, M. Wakeshima, Y. Hinatsu, T. Namiki, K. Takeda, I. Shirotani, H. Sugawara, D. Kikuchi, and H. Sato, J. Phys. Soc. Jpn. **78**, 124601 (2009).

[51] G. P. Meisner, G. R. Stewart, M. S. Torikachvili, and M. B. Maple, *Proceedings of the 17th International Conference of Low-Temperature Physics, edited by U. Eckern, A. Schmid, W. Weber, and W. Wühl* (Elsevier, Amsterdam, 1984) p. 711.

[52] G. Meisner, Physica B+C **108**, 763 (1981).

[53] Y. Iwahashi, H. Sugawara, K.-i. Magishi, T. Saito, K. Koyama, R. Settai, Y. Ōnuki, G. Giester, and P. Rogl, J. Phys. Soc. Jpn. **77**, 219 (2008).

[54] J. Juraszek, Z. Henkie, and T. Cichorek, Acta Phys. Pol. A **130**, 597 (2016).

[55] J. Singleton, P.-C. Ho, M. B. Maple, H. Harima, P. A. Goddard, and Z. Henkie, Physica B **403**, 758 (2008).

[56] N. Takeda and M. Ishikawa, J. Phys. Soc. Jpn. **69**, 868 (2000).

[57] H. Harima and K. Takegahara, Physica C **388-389**, 555 (2003).

[58] M. E. Danebrock, C. B. H. Evers, and W. Jeitschko, J. Phys. Chem. Solids **57**, 381 (1996).

[59] K.-i. Magishi, Y. Nakai, K. Ishida, H. Sugawara, I. Mori, T. Saito, and K. Koyama, J. Phys. Soc. Jpn. **75**, 023701 (2006).

[60] S. Tatsuoka, H. Sato, K. Tanaka, M. Ueda, D. Kikuchi, H. Aoki, T. Ikeno, K. Kuwahara, Y. Aoki, H. Sugawara, and H. Harima, J. Phys. Soc. Jpn. **77**, 033701 (2008).

[61] H. Harima and K. Takegahara, Physica B **328**, 26 (2003).

[62] I. Shirotani, S. Sato, C. Sekine, K. Takeda, I. Inagawa, and T. Yagi, J. Phys.: Condens. Matter **17**, 7353 (2005).